APPLIED PHYSICS

Room temperature polariton lasing in quantum heterostructure nanocavities

Jang-Won Kang[1], Bokyung Song[1], Wenjing Liu[2], Seong-Ju Park[3], Ritesh Agarwal[2]*, Chang-Hee Cho[1]*

Ultralow-threshold coherent light emitters can be achieved through lasing from exciton-polariton condensates, but this generally requires sophisticated device structures and cryogenic temperatures. Polaritonic nanolasers operating at room temperature lie on the crucial path of related research, not only for the exploration of polariton physics at the nanoscale but also for potential applications in quantum information systems, all-optical logic gates, and ultralow-threshold lasers. However, at present, progress toward room temperature polariton nanolasers has been limited by the thermal instability of excitons and the inherently low quality factors of nanocavities. Here, we demonstrate room temperature polaritonic nanolasers by designing wide-gap semiconductor heterostructure nanocavities to produce thermally stable excitons coupled with nanocavity photons. The resulting mixed states of exciton polaritons with Rabi frequencies of approximately 370 meV enable persistent polariton lasing up to room temperature, facilitating the realization of miniaturized and integrated polariton systems.

INTRODUCTION

Lasing from exciton-polariton condensates in solid-state systems is distinguished from conventional lasing by the exhibition of low-threshold polariton lasing with macroscopic and spontaneous coherence (*1*–*5*). Strong coupling between excitons and photons is crucial for the formation of the bosonic quasiparticles known as exciton polaritons, which is generally achieved by means of two-dimensional (2D) semiconductor quantum wells (QWs) embedded in high-finesse optical microcavities (*1*, *4*, *5*). Despite the design of elaborate structures to obtain high-quality excitons and cavity photons, polariton lasing has mostly been observed at cryogenic temperatures due to the small binding energies (~10 meV) of Wannier-Mott excitons in typical semiconductors (*4*, *5*). With wide-gap semiconductors of larger exciton binding energies such as GaN (~20 meV) and ZnO (~60 meV), room temperature polariton lasing has been recently achieved under both optical and electrical injections (*6*–*12*). Moreover, organic (*13*) and polymer (*14*) materials have also shown polariton condensation and lasing at room temperature owing to the large binding energy (~1 eV) of Frenkel excitons.

In particular, ZnO is a promising semiconducting material to realize room temperature polariton devices due to the large exciton binding energy exceeding the thermal energy. High-quality ZnO coupled with planar microcavities has been studied to demonstrate strong coupling and room temperature polariton lasers (*8*, *10*). Single-crystalline ZnO microwires, which support whispering gallery cavity modes with a high quality factor, have shown polariton lasing even at higher temperatures than room temperature (*11*). Moreover, a 1D polariton superlattice has been realized using the ZnO microwire laying on a grating structure, providing an engineered polariton state (*12*).

The coupling strength between excitons and cavity photons scales as $\Omega \sim \sqrt{(f/V_m)}$, where Ω is the Rabi frequency, f is the oscillator strength of the excitons, and V_m is the mode volume of the cavities (*3*). Semiconducting nanostructures such as nanorods simultaneously produce excitons and cavity photons with reduced mode volumes, boosting their interaction time and, thus, the coupling strength. Size-tunable and enhanced coupling strengths have been observed in semiconductor nanowire cavities, enabling strong coupling without high-finesse microcavities (*15*, *16*). The development of room temperature polaritonic nanolasers, however, is still limited by the thermal instability of the excitons and the inherently low quality factors of the nanocavities (*17*). A recent theoretical study has revealed that the lasing in nanocavities such as ZnO nanowires does not originate from exciton polaritons, but from electron-hole plasma at room temperature (*18*). In this regard, QW heterostructures integrated on the nanocavity may pave the way to achieve room temperature polariton lasing by enhancing the oscillator strength and thermal stability of the excitons beyond the bulk properties.

Here, we demonstrate room temperature polaritonic nanolasers of simple nanorod geometry by designing wide-gap semiconductor QW heterostructure nanocavities, each composed of a nanorod core enclosed by a radial QW shell. The radial QWs grown on the nonpolar plane (hexagonal facets) are free from quantum-confined Stark effect, leading to enhanced oscillator strength and exciton binding energy (*19*, *20*). Spectroscopic measurements reveal that the oscillator strength and thermal stability are greatly enhanced for the radial QW excitons compared with the bulk excitons. Thus, the radial QW structure enables strong coupling with photons confined in a small-mode-volume (0.1 μm^3) nanocavity, giving rise to Rabi frequencies of ~370 meV at room temperature. Our unique approach exploits these quantum heterostructure nanocavities to enable persistent polariton lasing up to room temperature. Furthermore, a double threshold behavior well below and above the Mott density, observed in quantum heterostructure nanocavities, evidences the transition from polariton to photon lasing regimes.

RESULTS

Quantum heterostructure nanocavity

The quantum heterostructure nanocavity used in this study consists of a ZnO nanorod core and a multi-QW shell with five pairs of a 4-nm-thick

[1]Department of Emerging Materials Science, Daegu Gyeongbuk Institute of Science and Technology (DGIST), Daegu 42988, South Korea. [2]Department of Materials Science and Engineering, University of Pennsylvania, Philadelphia, PA 19104, USA. [3]School of Materials Science and Engineering, Gwangju Institute of Science and Technology, Gwangju 61005, South Korea.
*Corresponding author. Email: chcho@dgist.ac.kr (C.-H.C.); riteshag@seas.upenn.edu (R.A.)

ZnO QW layer and a 10-nm-thick $Zn_{0.9}Mg_{0.1}O$ barrier layer, as shown schematically in Fig. 1A. The radial QW structure is grown on an array of ZnO cores by means of metal-organic chemical vapor deposition (MOCVD) (see Materials and Methods). Figure 1B presents a scanning electron microscopy (SEM) image of an as-grown QW nanorod array, with an average rod diameter of ~600 nm and a rod length of ~2.7 μm, which belongs to a waveguide structure to support Fabry-Pérot cavity modes along the axial direction over the emission wavelength range of ZnO QWs. The conformal growth of single-crystalline radial QWs is confirmed by radial cross-sectional scanning transmission electron microscopy (STEM) images (Fig. 1, C and D), which show the five-period QW and barrier layers. Note that the QW nanorod depicted in Fig. 1 (C and D) was encapsulated with an additional ZnO layer to obtain high-contrast STEM images of the QW region. Structural analysis via axial cross-sectional energy-dispersive x-ray spectroscopy, as shown in Fig. 1E, further confirms the highly conformal growth of the QW layers.

To investigate the exciton properties of the QW nanorods, spatially resolved micro–photoluminescence (PL) measurements were performed on single QW nanorods transferred onto an SiO_2/Si substrate. Figure 1F presents the exciton luminescence spectrum of a single ZnO QW nanorod in comparison with that of a bare ZnO nanorod (without QWs), where each spectrum was measured at the center of the nanorod under continuous-wave 325-nm laser excitation with a low pump power density of 0.67 kW/cm^2 at room temperature. Compared with the bare nanorod, which exhibits an emission peak at ~3.26 eV with a full width at half maximum (FWHM) of 88 meV, the QW nanorod shows an exciton emission intensity that is much stronger and peaks at ~3.32 eV with an FWHM of 58 meV. The observed PL peak (~3.26 eV) for the bare nanorod corresponds to the first longitudinal optical (LO) phonon replica of free A exciton (3.306 eV) due to strong exciton–LO phonon coupling in the bulk ZnO (*21*). However, the PL peak (~3.32 eV) for the QW nanorod is primarily dominated by zero-phonon excitonic

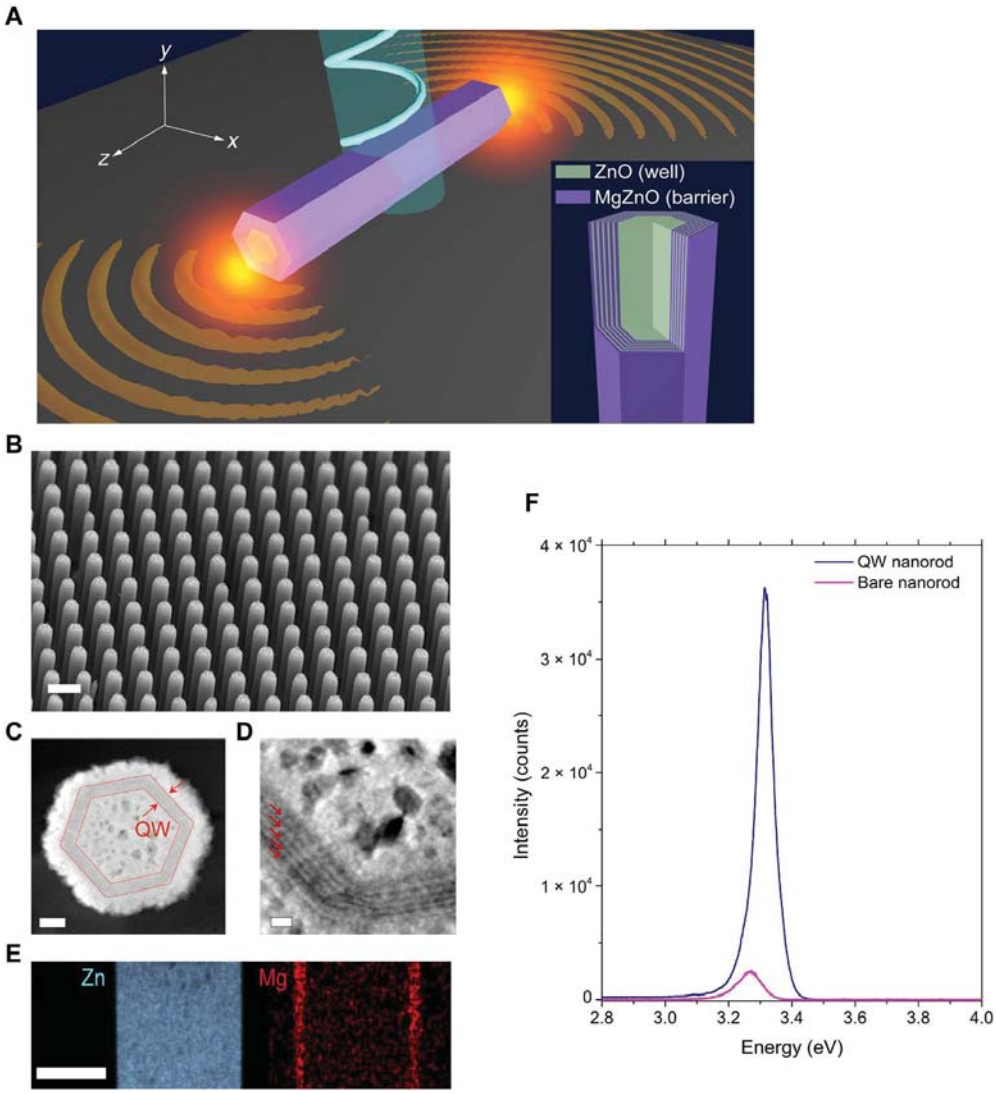

Fig. 1. Quantum heterostructure nanocavities. (**A**) Schematic illustration of a single nanorod polariton laser on an SiO_2 substrate. The inset shows the shell structure, consisting of five pairs of $Zn_{0.9}Mg_{0.1}O$/ZnO QW layers. (**B**) SEM image of an as-grown QW nanorod array with an average rod diameter of ~600 nm and a rod length of ~2.7 μm. Scale bar, 1 μm. (**C**) STEM image showing a radial cross section of a QW nanorod. Scale bar, 100 nm. (**D**) Magnified STEM image of the QW region. The arrows indicate the ZnO wells. Scale bar, 20 nm. Note that the QW nanorod depicted in (C) and (D) was encapsulated with an additional ZnO layer to obtain high-contrast images of the QW region. (**E**) Elemental mapping images of an axial cross section of a QW nanorod, showing the conformal growth of QW layers on the core ZnO nanorod. Scale bar, 300 nm. (**F**) Exciton luminescence spectrum of a single QW nanorod at room temperature compared with the spectrum of a bare nanorod.

emission because the coupling between the exciton and LO phonon is greatly reduced in QW structures (*22*, *23*). This results in the quantum confinement energy of ~14 meV, which is further confirmed in low-temperature reflectance measurements at 5 K (section S1) and also consistent with the theoretical calculations (*24*). Reflectance measurements also identified the enhanced oscillator strength in the radial QWs by a factor of 2 for A and B excitons compared with that of bulk (section S1). The observed blueshift, enhanced intensity, and reduced broadening of the exciton emission peak from the QW nanorod originate from quantum confinement effects (*24*, *25*), indicating that the radial QW structure provides thermally stable excitons with an enhanced oscillator strength even at room temperature (section S1).

Exciton-polariton dispersion

The formation of exciton polaritons and their coupling strengths in waveguide geometries can be analyzed by measuring the waveguided PL at one end of a nanorod when the other end of the nanorod is excited with a focused laser spot (see Materials and Methods). Note that a low level of excitation (0.67 kW/cm^2) was used to create an exciton density (8.8×10^{16} cm^{-3}) well below the Mott density (1.5×10^{18} cm^{-3}) because above the Mott density, the excitons dissociate into an electron-hole plasma (*17*, *18*). Strong coupling between the excitons and cavity photons in a QW nanorod gives rise to coupled eigenstates consisting of upper and lower polariton branches with a vacuum Rabi frequency (Ω) (*26*), which is the frequency of the oscillation between the exciton and photon states. Figure 2A presents the PL spectra at room temperature, measured at the end and the body (center) of a QW nanorod with a diameter of 640 nm and a length of 2.75 μm. The body emission is dominated by a Lorentzian-shaped single peak centered at ~3.32 eV, which is attributed to the emission from QW excitons. In contrast, the end emission is composed of the weak shoulder peak at ~3.32 eV on the higher-energy side and the strong emission at ~3.20 eV on the lower-energy side. The weak shoulder peak of the end emission, which corresponds to the body emission peak, results from the detection of uncoupled-exciton emission due to the short distance between the excitation and detection spots. The strong emission centered at ~3.20 eV on the lower-energy side is assigned to the emission from the lower polariton branch. The strong and broad emission from the lower polariton branch reveals clear multiple resonance peaks, resulting from the eigenmodes of the exciton polaritons, which are composite quasiparticles consisting of the QW excitons and the Fabry-Pérot cavity photons in the QW nanorod. From the resonance peaks, the cavity Q-factor is estimated to be ~150. By fitting the measured resonance peaks to the theoretical model for 1D exciton-polariton waveguide modes, the energy-momentum (E-k_z) dispersion of the exciton polaritons along the long axis of the ZnO QW nanorod can be obtained (*16*, *27*). Figure 2B presents the E-k_z dispersion of the exciton polaritons for a ZnO QW nanorod with a diameter of 640 nm and a length of 2.75 μm. Note that the data points represent measured resonance energies with equidistant momenta at integer values of π/L_z, where L_z is the length of the nanorod. To determine the dominant cavity modes that are valid for the observed exciton-polariton eigenmodes, we numerically calculated the electromagnetic fields in the nanorod cavity using a finite-difference time domain method (section S2). The calculated results indicate that the dominant cavity modes in the QW nanorod are HE_{22} and HE_{13}. Then, the E-k_z relation was calculated using the theoretical model for 1D exciton-polariton waveguide dispersion (section S3). The experimentally measured resonance energies with equidistant momenta at the interval of π/L_z were fitted to the calculated E-k_z polariton dispersion by a parallel shift of the data points in the momentum axis. Note that the initial values of the equidistant momenta can be roughly estimated by simulating the field distribution of the Fabry-Pérot cavity mode since $k_z = n\pi/L_z$,

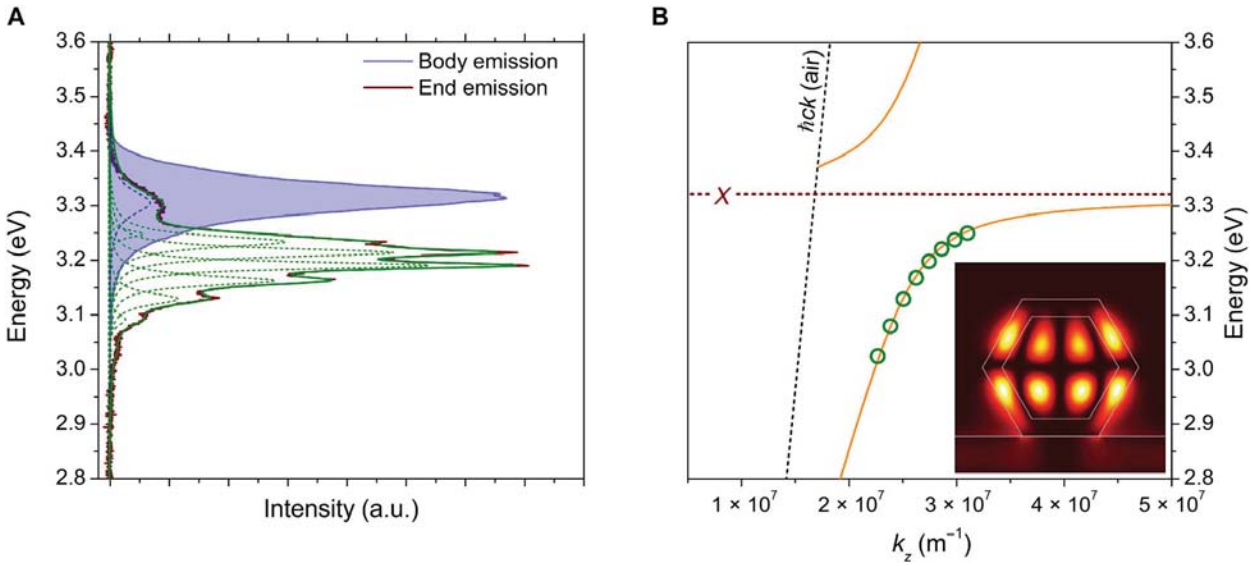

Fig. 2. Polariton dispersion at room temperature. (**A**) Excitonic (blue line) and waveguided (red line) PL spectra from the body center and end of a QW nanorod (diameter, 640 nm; length, 2.75 μm), respectively. The end emission exhibits multiple resonance peaks, which correspond to the eigenmodes of the exciton polaritons in the quantum heterostructure nanocavity. The dashed green lines represent the fitted Lorentzian line shapes used to determine the resonance energies in the lower polariton branch. The overall fitting line is displayed by the green line. The measurements were conducted using the 325-nm continuous-wave laser excitation at the power density of 670 W/cm^2 for the acquisition time of 60 s. (**B**) Dispersion relation of the exciton polaritons along the long axis of the QW nanorod. The data points represent measured resonance energies with equidistant momenta at integer values of π/L_z, where L_z is the length of the nanorod. The orange solid line represents the fit to the theoretical model for the exciton polariton HE_{22}-guided mode, indicating an estimated Rabi splitting energy of ~370 meV. The horizontal red dashed line represents the QW exciton energy. The inset shows the calculated electric field intensity ($|E_y|^2$) profile in the radial cross-sectional plane for the HE_{22}-guided mode at an energy of 3.20 eV, where white lines indicate the QW region. a.u., arbitrary units.

where n is the number of antinodes along the z axis (section S2). The oscillator strength was also adjusted as a fit parameter. Last, an excellent fit was obtained with the enhanced oscillator strength of the QW excitons by a factor of 2 compared with the bulk excitons when the QW excitons are coupled to the HE_{22} cavity mode (inset of Fig. 2B). The E-k_z dispersion of the exciton polaritons for the ZnO QW nanorod confirms the strong coupling with a Rabi splitting energy ($\hbar\Omega$) of ~370 meV.

Such a large Rabi splitting energy ($\hbar\Omega$) in the QW nanorods results from the enhanced oscillator strength of QW excitons and the reduced mode volume of nanocavity (*3*). In section S1, the reflectance measurements show that the longitudinal-transverse splitting ($\hbar\omega_{LT}$) for the QW excitons is about 24 meV, indicating that the oscillator strength ($f \approx 2\omega_{LT}\omega_T$) of the QW excitons is enhanced by a factor of 2, compared with that of the bulk A and B excitons (*28*, *29*). Taking into account the enhanced oscillator strength, the mode volume (0.1 μm^{-3}), and the spatial overlap (0.23) between the field and the QWs (*16*, *19*, *30*), the Rabi splitting energy ($\hbar\Omega$) was calculated to be about 374 meV, which is in excellent agreement with the value obtained from the polariton dispersion (section S4).

Room temperature lasing characteristics

To investigate the lasing characteristics of ZnO QW nanorods at room temperature, micro-PL measurements were conducted for individual QW nanorods under 355 nm pulsed excitation at various pump fluences (see Materials and Methods). Figure 3A shows an SEM image of a single ZnO QW nanorod transferred onto an SiO_2/Si substrate. Figure 3 (B to E) presents optical images showing a transition from spontaneous to coherent emission with increasing pump fluence. Above the lasing threshold, the typical interference patterns associated with longitudinal Fabry-Pérot cavity modes are observed from the QW nanorod (*31*). The interference pattern results from the coherent light emission from the two end facets of the nanorod, at which the light is emitted nearly spherically due to diffraction at the nanoscale apertures (*31*). This coherence in light emission is further evidenced by angle-resolved emission spectra showing the phase-correlated interference patterns (*32*), resembling Young's double-slit experiments, where the coherent light emitted from the two end facets of the nanorod interferes with each other (section S5). Figure 3F presents the micro-PL spectra of the ZnO QW nanorod at room temperature. At a pump fluence of 286 $\mu J/cm^2$, an abrupt increase in emission intensity is observed at the lasing peak energy of 3.225 eV, whereas broad spontaneous emission is observed below the lasing threshold. A remarkable feature is that the single-mode lasing near the threshold has an extremely narrow linewidth of 0.7 meV even at room temperature. Figure 3G shows the spectral map of the lasing behavior as a function of the pump fluence. A gradual blueshift of the single-mode lasing peak is observed with increasing pump fluence at the range below the Mott density (<810 $\mu J/cm^2$),

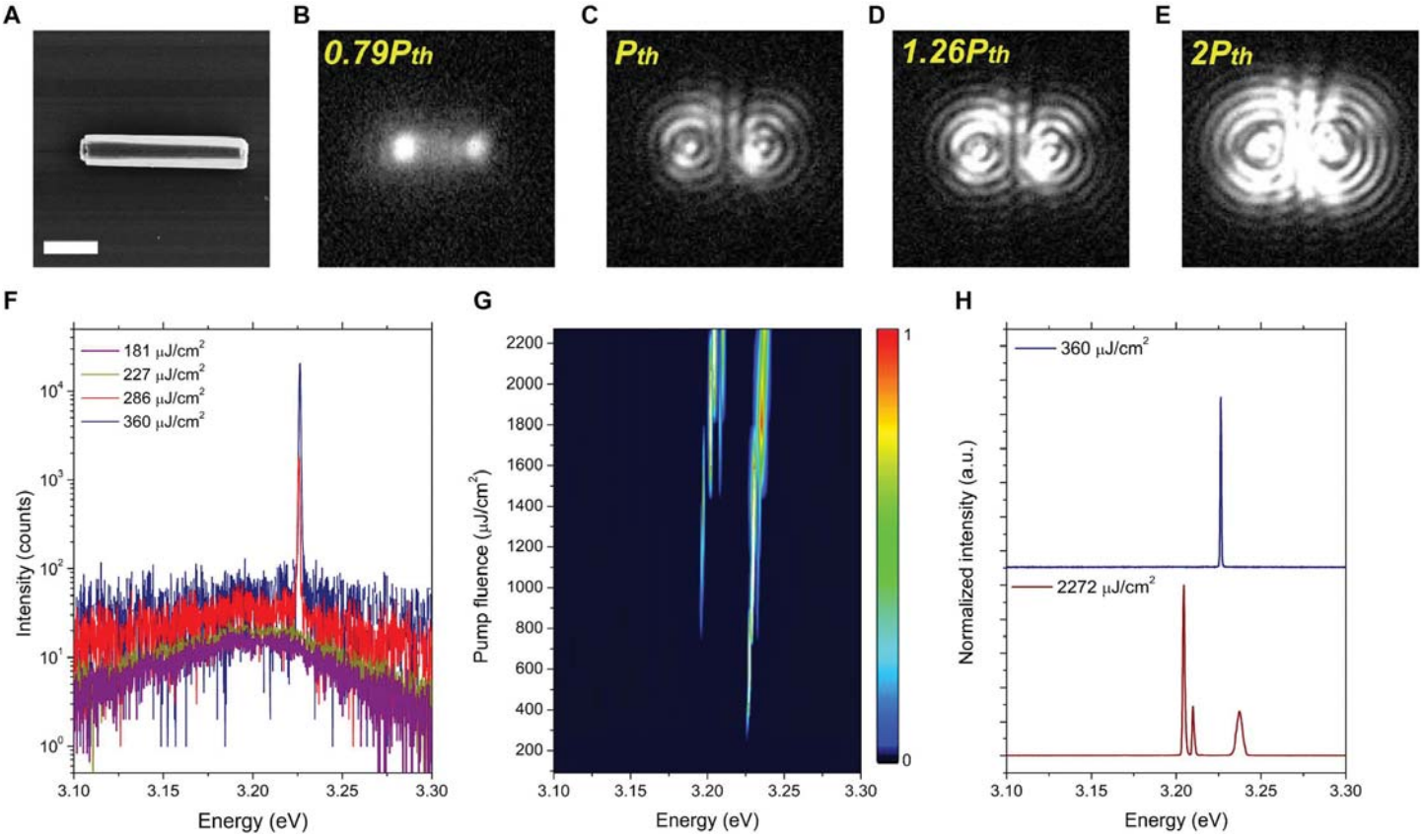

Fig. 3. Room temperature polariton lasing spectra. (**A**) SEM image of a single QW nanorod transferred onto an SiO_2/Si substrate. Scale bar, 1 μm. (**B** to **E**) Optical images showing a transition from spontaneous to coherent emission with increasing pump fluence. The interference patterns associated with longitudinal Fabry-Pérot cavity modes are observed. (**F**) Spectral evolution of a single QW nanorod laser (diameter of 580 nm and length of 2.70 μm) near the lasing threshold. All lasing spectra were collected using a 355-nm pulsed wave laser excitation at the power density of 180 to 360 mW/cm^2 for the acquisition time of 10 s. (**G**) Spectral map of the lasing behavior of the QW nanorod laser as a function of pump fluence. (**H**) Normalized emission spectra of the QW nanorod laser at low (360 $\mu J/cm^2$) and high (2272 $\mu J/cm^2$) pump fluences.

which results from the repulsive interactions between the polariton and the uncondensed exciton reservoir, and also between the polaritons (*33*). As the pump fluence is further increased above the Mott density (>810 μJ/cm^2), the system enters a weak coupling regime, and another lasing peak centered at ~3.195 eV emerges on the lower-energy side, which can be explained by the shift of gain regime, and relevant mode change to the lower energy side due to the bandgap renormalization at this higher level of excitation (*34*). With the gradual transition from excitons to electron-hole plasma, the additional blueshift of lasing peak occurs because of the reduction of exciton binding energy and change of refractive index (*34*). Figure 3H compares the lasing spectra at low (360 μJ/cm^2) and high (2272 μJ/cm^2) pump fluences, showing a marked change in the lasing mechanism as the pump fluence increases.

Polariton lasing essentially requires excitons to be strongly coupled with photons under above-threshold excitation. However, as the excitation increases, the exciton density also increases, and Coulomb screening reduces the binding energy of the excitons, causing the system to eventually enter the regime of an uncorrelated electron-hole plasma. The crucial density criterion separating the excitonic and electron-hole plasma regimes is the Mott density, where the experimentally measured value in bulk ZnO is 1.5×10^{18} cm^{-3} at room temperature (*18*, *35*). For an ideal 2D QW, the exciton Bohr radius is decreased to half of that of the equivalent 3D exciton (*36*), leading to higher Mott density for the 2D excitons. However, for the ZnO QWs used in this study, the Mott density would be slightly larger or similar with the value for bulk ZnO because the thickness of QW (4 nm) is larger than the exciton Bohr radius of bulk ZnO (~1.8 nm) (*17*). The Mott densities in realistic GaN and GaAs QWs are almost the same with those of the bulk counterparts (*37*–*40*). Thus, the Mott density of bulk ZnO is used for both the QW and bare nanorods to qualitatively compare their lasing characteristics.

Polariton lasing characteristics of QW nanocavities

To verify that the observed lasing action is due to the coherence of the exciton polaritons in the ZnO QW nanorods, we investigated the lasing characteristics with increasing electron-hole pair (EHP) densities by varying the excitation fluence. Figure 4A shows a double-logarithmic plot of the integrated intensity as a function of the incident pump fluence at room temperature, and the results confirm the clear threshold behavior of the lasing phenomenon. Notably, the ZnO QW nanorods exhibit a lasing threshold of 286 μJ/cm^2, which is much lower than the critical transition excitation of 810 μJ/cm^2 corresponding to the Mott density. Above the lasing threshold, the polariton dispersion is still maintained with a Rabi splitting energy ($\hbar\Omega$) of ~360 meV, indicating the polariton lasing occurs in a strong coupling regime (section S6). Moreover, the QW nanorods show the behavior characteristic of a second threshold above the critical excitation corresponding to the Mott density, where a transition from polariton to photon lasing occurs. This second threshold behavior evidences the transition from strong to weak coupling regime with the onset of photon lasing, as observed in GaAs-based low-dimensional microcavities (*41*, *42*). Together with the observed blueshift of the lasing peak (Fig. 3G), the second threshold behavior strongly supports that the lasing observed in the ZnO QW nanorods originates from strong coupling of the exciton polaritons. The double threshold behavior for the QW nanorods was observed reproducibly, as provided in the statistical data (section S7).

The same plot for bare ZnO nanorods is also displayed for comparison. A stark contrast can be seen from the fact that the lasing threshold of the bare ZnO nanorods appears at an excitation (905 μJ/cm^2) that is above the critical value corresponding to the Mott density, meaning that the lasing in the bare nanorods is photon lasing from the electron-hole plasma (section S8). Statistics on the lasing threshold for the bare nanorods are also provided in section S7. Figure 4B presents a double-logarithmic plot of the linewidth versus pump fluence. For both the QW and bare nanorods, the lasing linewidths are well below the linewidth associated with the calculated quality factor (<500) for the photonic cavity modes in the nanorod geometry. An important distinction is that for the QW nanorods, the sharp linewidth is maintained until the Mott density is reached, and the linewidth then gradually increases as the system enters the photon lasing regime, whereas for the bare nanorods, a simple increase is seen in the linewidth of the lasing peak due to the change in the refractive index associated with the electron-hole plasma (*43*). To further investigate the lasing behavior in relation to excitation, we measured the EHP density at the threshold, as obtained from the measured threshold pump fluence, in the temperature range from 77 to 297 K. Note that the threshold EHP density per QW was estimated using the net absorption in the QW structure calculated via transfer matrix methods (section S9). Figure 4C plots the threshold EHP density as a function of temperature for both the QW nanorods and the bare nanorods. For the QW nanorods, the threshold EHP density is as low as 4.5×10^{16} cm^{-3} at 77 K and slowly increases with increasing temperature, up to 2.8×10^{17} cm^{-3} at room temperature (297 K); all of the values over the entire temperature range are well below the Mott density of 1.5×10^{18} cm^{-3}. By contrast, the bare nanorods show a much more rapid increase in the threshold EHP density with increasing temperature; the threshold density eventually exceeds the Mott density above 257 K and reaches a value of 3.2×10^{18} cm^{-3} at room temperature. Figure 4D presents the temperature-dependent evolution of the lasing mode for the QW nanorods. The data show the gradual redshift of a given lasing mode with increasing temperature due to the temperature-induced shift of the exciton energy (yellow dashed line). In addition, the successive mode change is observed over the wide temperature range of 77 to 297 K, resulting from the discrete and narrow distribution of polariton eigenmodes in the QW nanorods. Note that the mode spacing of polaritons is much smaller than that of the cavity photons (white dotted line) due to the avoided crossing of the exciton and photon dispersions. The lasing mode change is closely correlated with the relaxation and population mechanisms of the exciton polaritons. The energy separation between the lasing mode and the exciton resonance corresponds to the LO phonon energy of ~72 meV (*17*), implying that the population of the polariton eigenmodes is dominated by LO phonon relaxation from the exciton reservoir (*44*). By contrast, the lasing mode of the bare nanorods appears near or above the exciton resonance energy in the temperature range of 267 to 297 K as a result of the photon lasing in the electron-hole plasma regime (section S10). These results highlight the crucial role of quantum heterostructures in the realization of room temperature polariton lasing in single nanostructures.

DISCUSSION

We have successfully demonstrated room temperature exciton polariton lasing in quantum heterostructure nanocavities. By virtue of the thermal stability, enhanced oscillator strength, and strong coupling with cavity photons of the QW excitons, such a quantum heterostructure nanocavity shows persistent exciton polariton lasing up to room temperature. The polariton lasing is confirmed with large Rabi splitting energies in 1D exciton polariton dispersion relations. The double threshold behavior well below and above the Mott density, observed in the quantum

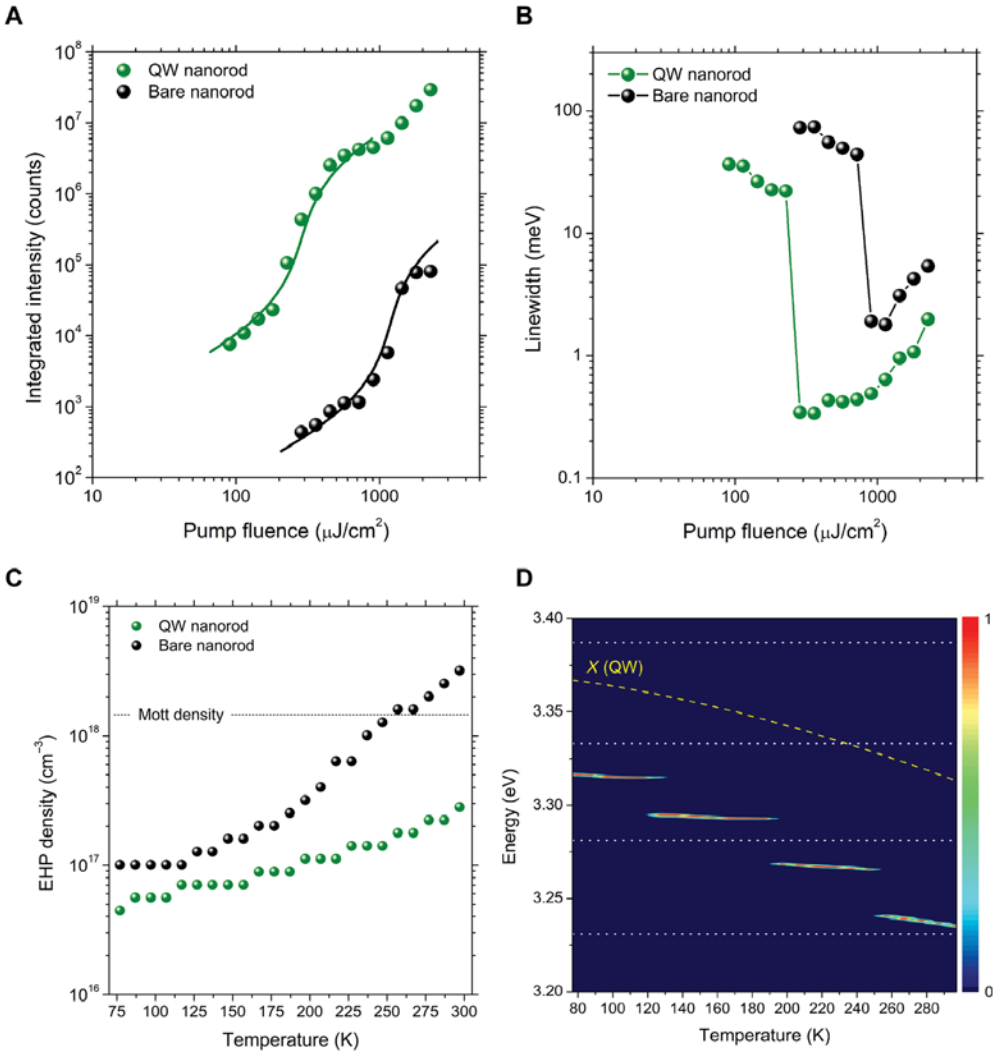

Fig. 4. Density and temperature dependence of polariton lasing. (**A** and **B**) Double-logarithmic plots of integrated intensity (**A**) and linewidth (**B**) as a function of pump fluence at room temperature for a QW nanorod and a bare nanorod, showing the clear threshold behavior of the lasing. (**C**) EHP density at the threshold pump fluence in the temperature range from 77 to 297 K for both the QW and bare nanorods. The horizontal dotted line indicates the Mott density of ZnO at room temperature. (**D**) Spectral map of the QW nanorod laser measured in the temperature range from 77 to 297 K, showing the temperature-dependent evolution of the lasing mode. The yellow dashed line represents the temperature-dependent exciton energy of the QW nanorod. The white dotted lines indicate the pure photon modes of Fabry-Pérot cavity resonances for the QW nanorod.

heterostructure nanocavities, evidences the transition from polariton to photon lasing regimes. Our demonstration opens up the possibility of studying various intriguing polaritonic phenomena in nanoscale systems and enables the realization of efficient nanolasers, all-optical logic gates, and quantum computing devices operating at room temperature.

MATERIALS AND METHODS

Device fabrication

Quantum heterostructure nanocavities were fabricated via a two-step growth procedure. First, ZnO nanorod arrays were synthesized using a patterned nanohole photoresist mask on ZnO (200 nm)/sapphire substrates by means of a hydrothermal method using an aqueous solution of equimolar zinc nitrate hydrate and hexamethylene-tetramine. Then, five pairs of ZnMgO/ZnO layers were grown on the core ZnO nanorods using a shower head–type MOCVD reactor equipped with computer-controlled gas flow systems. Diethylzinc (DEZn), bis(cyclopentadienyl) magnesium (CP_2Mg), and O_2 gas were used as sources of Zn, Mg, and O, respectively. Ar was used as the carrier gas. $Zn_{0.9}Mg_{0.1}O$ was grown at 810°C and a CP_2Mg-to-DEZn flow ratio of 0.2. The growth conditions for high-quality QW structures were optimized by controlling the (DEZn + CP_2Mg)/O_2 ratio.

Optical measurements

The as-grown nanocavities were dry transferred onto 400-nm-thick SiO_2-coated Si substrates for optical measurements performed using a home-built microscope equipped with objectives (Nikon). The excitation power was adjusted using neutral density filters. For spatially resolved micro-PL spectroscopy, a continuous-wave 325-nm He-Cd laser (Kimmon Koha) was focused by an objective [60×, 0.7 numerical aperture (NA)] to a beam spot size of ~3 μm with a power density range of 0.67 to 2.2 kW/cm^2, corresponding to an estimated excited EHP density of 8.8×10^{16} to 3.5×10^{17} cm^{-3}. PL spectra were collected using the same objective and an optical fiber on the focal image plane, resulting in

a spatial resolution of less than 300 nm. The signal collected by the optical fiber was coupled to a 0.5-m spectrometer (Acton) and a cooled charge-coupled device (Pixis 2K, Princeton Instruments) with a spectral resolution of 0.1 nm. The lasing characteristics of the nanocavities were examined using the same optical setup but with excitation by a pulsed-wave 355-nm laser (Teem Photonics) with a repetition rate of 1 kHz and a pulse width of 350 ps, which was focused by a 20×, 0.45 NA objective to a beam spot size of ~14 μm. Temperature-dependent measurements were conducted using a liquid nitrogen–cooled cryostat (Janis Research).

SUPPLEMENTARY MATERIALS

Supplementary material for this article is available at http://advances.sciencemag.org/cgi/content/full/5/4/eaau9338/DC1

Section S1. Oscillator strength in bare and QW nanorods
Section S2. Numerical simulation of the Fabry-Pérot cavity modes
Section S3. Polariton dispersion curves with guided modes in the QW nanorod cavity
Section S4. Rabi splitting energy in the QW nanorod cavity
Section S5. Angle-resolved emission spectra from the QW nanorod and spatial coherence
Section S6. Polariton dispersion above lasing threshold density
Section S7. Statistical data for lasing thresholds
Section S8. Room temperature lasing spectra of the bare ZnO nanorod cavity
Section S9. Estimation of EHP density in bare and QW nanorods
Section S10. Temperature-dependent lasing characteristics of the bare ZnO nanorod
Fig. S1. Reflectance spectra of bare and QW nanorods at 5 K.
Fig. S2. Electric field distribution for HE_{22} and HE_{13} waveguide modes in the nanorod cavity geometry.
Fig. S3. Polariton dispersion curves.
Fig. S4. Angle-resolved emission spectra from the QW nanocavity.
Fig. S5. Photoluminescence spectra and polariton dispersion at the exciton density above the lasing threshold.
Fig. S6. Statistical data of the lasing threshold for QW and bare nanorods.
Fig. S7. Emission spectra of the bare ZnO nanorod cavity depending on the pump fluence.
Fig. S8. Absorption spectra for ZnO and $Zn_{0.9}Mg_{0.1}O$ layers.
Fig. S9. Temperature-dependent lasing spectra of the bare ZnO nanorod.
References (*45*–*50*)

REFERENCES AND NOTES

1. J. Kasprzak, M. Richard, S. Kundermann, A. Baas, P. Jeambrun, J. M. J. Keeling, F. M. Marchetti, M. H. Szymańska, R. André, J. L. Staehli, V. Savona, P. B. Littlewood, B. Deveaud, S. Dang le, Bose–Einstein condensation of exciton polaritons. *Nature* **443**, 409–414 (2006).
2. D. Sanvitto, S. Kéna-Cohen, The road towards polaritonic devices. *Nat. Mater.* **15**, 1061–1073 (2016).
3. J. P. Reithmaier, G. Sęk, A. Löffler, C. Hofmann, S. Kuhn, S. Reitzenstein, L. V. Keldysh, V. D. Kulakovskii, T. L. Reinecke, A. Forchel, Strong coupling in a single quantum dot–semiconductor microcavity system. *Nature* **432**, 197–200 (2004).
4. H. Deng, G. Weihs, D. Snoke, J. Bloch, Y. Yamamoto, Polariton lasing vs. photon lasing in a semiconductor microcavity. *Proc. Natl. Acad. Sci. U.S.A.* **100**, 15318–15323 (2003).
5. C. Schneider, A. Rahimi-Iman, N. Y. Kim, J. Fischer, I. G. Savenko, M. Amthor, M. Lermer, A. Wolf, L. Worschech, V. D. Kulakovskii, I. A. Shelykh, M. Kamp, S. Reitzenstein, A. Forchel, Y. Yamamoto, S. Höfling, An electrically pumped polariton laser. *Nature* **497**, 348–352 (2013).
6. A. Das, J. Heo, M. Jankowski, W. Guo, L. Zhang, H. Deng, P. Bhattacharya, Room temperature ultralow threshold gan nanowire polariton laser. *Phys. Rev. Lett.* **107**, 066405 (2011).
7. G. Christmann, R. Butté, E. Feltin, J.-F. Carlin, N. Grandjean, Room temperature polariton lasing in a GaN⁄AlGaN multiple quantum well microcavity. *Appl. Phys. Lett.* **93**, 051102 (2008).
8. F. Li, L. Orosz, O. Kamoun, S. Bouchoule, C. Brimont, P. Disseix, T. Guillet, X. Lafosse, M. Leroux, J. Leymarie, M. Mexis, M. Mihailovic, G. Patriarche, F. Réveret, D. Solnyshkov, J. Zuniga-Perez, G. Malpuech, From excitonic to photonic polariton condensate in a ZnO-based microcavity. *Phys. Rev. Lett.* **110**, 196406 (2013).
9. P. Bhattacharya, T. Frost, S. Deshpande, M. Z. Baten, A. Hazari, A. Das, Room temperature electrically injected polariton laser. *Phys. Rev. Lett.* **112**, 236802 (2014).
10. F. Li, L. Orosz, O. Kamoun, S. Bouchoule, C. Brimont, P. Disseix, T. Guillet, X. Lafosse, M. Leroux, J. Leymarie, G. Malpuech, M. Mexis, M. Mihailovic, G. Patriarche, F. Réveret, D. Solnyshkov, J. Zuniga-Perez, Fabrication and characterization of a room-temperature ZnO polariton laser. *Appl. Phys. Lett.* **102**, 191118 (2013).
11. D. Xu, W. Xie, W. Liu, J. Wang, L. Zhang, Y. Wang, S. Zhang, L. Sun, X. Shen, Z. Chen, Polariton lasing in a ZnO microwire above 450 K. *Appl. Phys. Lett.* **104**, 082101 (2014).
12. L. Zhang, W. Xie, J. Wang, A. Poddubny, J. Lu, Y. Wang, J. Gu, W. Liu, D. Xu, X. Shen, Y. G. Rubo, B. L. Altshuler, A. V. Kavokin, Z. Chen, Weak lasing in one-dimensional polariton superlattices. *Proc. Natl. Acad. Sci. U.S.A.* **112**, E1516–E1519 (2015).
13. S. Kéna-Cohen, S. R. Forrest, Room-temperature polariton lasing in an organic single-crystal microcavity. *Nat. Photonics* **4**, 371–375 (2010).
14. J. D. Plumhof, T. Stöferle, L. Mai, U. Scherf, R. F. Mahrt, Room-temperature Bose–Einstein condensation of cavity exciton–polaritons in a polymer. *Nat. Mater.* **13**, 247–252 (2014).
15. L. K. van Vugt, S. Rühle, P. Ravindran, H. C. Gerritsen, L. Kuipers, D. Vanmaekelbergh, Exciton polaritons confined in a ZnO nanowire cavity. *Phys. Rev. Lett.* **97**, 147401 (2006).
16. L. K. van Vugt, B. Piccione, C.-H. Cho, P. Nukala, R. Agarwal, One-dimensional polaritons with size-tunable and enhanced coupling strengths in semiconductor nanowires. *Proc. Natl. Acad. Sci. U.S.A.* **108**, 10050–10055 (2011).
17. C. Klingshirn, R. Hauschild, J. Fallert, H. Kalt, Room-temperature stimulated emission of ZnO: Alternatives to excitonic lasing. *Phys. Rev. B* **75**, 115203 (2007).
18. M. A. M. Versteegh, D. Vanmaekelbergh, J. I. Dijkhuis, Room-temperature laser emission of ZnO nanowires explained by many-body theory. *Phys. Rev. Lett.* **108**, 157402 (2012).
19. S.-H. Gong, S.-M. Ko, M.-H. Jang, Y.-H. Cho, Giant rabi splitting of whispering gallery polaritons in GaN/InGaN core-shell wire. *Nano Lett.* **15**, 4517–4524 (2015).
20. L. Béaur, T. Bretagnon, C. Brimont, T. Guillet, B. Gil, D. Tainoff, M. Teisseire, J.-M. Chauveau, Low temperature reflectivity study of nonpolar ZnO/(Zn,Mg)O quantum wells grown on M-plane ZnO substrates. *Appl. Phys. Lett.* **98**, 101913 (2011).
21. L. Wang, N. C. Giles, Temperature dependence of the free-exciton transition energy in zinc oxide by photoluminescence excitation spectroscopy. *J. Appl. Phys.* **94**, 973–978 (2003).
22. T. Makino, C. H. Chia, N. T. Tuan, H. D. Sun, Y. Segawa, M. Kawasaki, A. Ohtomo, K. Tamura, H. Koinuma, Room-temperature luminescence of excitons in ZnO/(Mg, Zn)O multiple quantum wells on lattice-matched substrates. *Appl. Phys. Lett.* **77**, 975 (2000).
23. H. D. Sun, T. Makino, Y. Segawa, M. Kawasaki, A. Ohtomo, K. Tamura, H. Koinuma, Enhancement of exciton binding energies in ZnO/ZnMgO multiquantum wells. *J. Appl. Phys.* **91**, 1993–1997 (2002).
24. G. Coli, K. K. Bajaj, Excitonic transitions in ZnO/MgZnO quantum well heterostructures. *Appl. Phys. Lett.* **78**, 2861–2863 (2001).
25. E.-S. Jang, J. Y. Bae, J. Yoo, W. I. Park, D.-W. Kim, G.-C. Yi, T. Yatsui, M. Ohtsu, Quantum confinement effect in ZnO⁄$Mg_{0.2}Zn_{0.8}O$ multishell nanorod heterostructures. *Appl. Phys. Lett.* **88**, 023102 (2006).
26. G. Khitrova, H. M. Gibbs, M. Kira, S. W. Koch, A. Scherer, Vacuum Rabi splitting in semiconductors. *Nat. Phys.* **2**, 81–90 (2006).
27. L. K. van Vugt, B. Piccione, R. Agarwal, Incorporating polaritonic effects in semiconductor nanowire waveguide dispersion. *Appl. Phys. Lett.* **97**, 061115 (2010).
28. L. Sun, Z. Chen, Q. Ren, K. Yu, L. Bai, W. Zhou, H. Xiong, Z. Q. Zhu, X. Shen, Direct observation of whispering gallery mode polaritons and their dispersion in a ZnO tapered microcavity. *Phys. Rev. Lett.* **100**, 156403 (2008).
29. C. Klingshirn, J. Fallert, H. Zhou, J. Sartor, C. Thiele, F. Maier-Flaig, D. Schneider, H. Kalt, 65 years of ZnO research - old and very recent results. *Phys. Status Solidi B* **247**, 1424–1447 (2010).
30. M. Zamfirescu, A. Kavokin, B. Gil, G. Malpuech, M. Kaliteevski, ZnO as a material mostly adapted for the realization of room-temperature polariton lasers. *Phys. Rev. B* **65**, 161205(R) (2002).
31. L. K. van Vugt, S. Rühle, D. Vanmaekelbergh, Phase-correlated nondirectional laser emission from the end facets of a ZnO nanowire. *Nano Lett.* **6**, 2707–2711 (2006).
32. L. Sun, M.-L. Ren, W. Liu, R. Agarwal, Resolving parity and order of Fabry–Pérot modes in semiconductor nanostructure waveguides and lasers: Young's interference experiment revisited. *Nano Lett.* **14**, 6564–6571 (2014).
33. L. Ferrier, E. Wertz, R. Johne, D. D. Solnyshkov, P. Senellart, I. Sagnes, A. Lemaître, G. Malpuech, J. Bloch, Interactions in confined polariton condensates. *Phys. Rev. Lett.* **106**, 126401 (2011).
34. J. Fallert, F. Stelzl, H. Zhou, A. Reiser, K. Thonke, R. Sauer, C. Klingshirn, H. Kalt, Lasing dynamics in single ZnO nanorods. *Opt. Express* **16**, 1125–1131 (2008).
35. M. A. M. Versteegh, T. Kuis, H. T. C. Stoof, J. I. Dijkhuis, Ultrafast screening and carrier dynamics in ZnO: Theory and experiment. *Phys. Rev. B* **84**, 035207 (2011).
36. E. Hanamura, Exciton enhancement of optical non-linearity in low-dimensional crystals. *Opt. Quant. Electron.* **21**, 441–450 (1989).
37. F. Binet, J. Y. Duboz, J. Off, F. Scholz, High-excitation photoluminescence in GaN: Hot-carrier effects and the Mott transition. *Phys. Rev. B* **60**, 4715–4722 (1999).
38. G. Rossbach, J. Levrat, G. Jacopin, M. Shahmohammadi, J.-F. Carlin, J.-D. Ganière, R. Butté, B. Deveaud, N. Grandjean, High-temperature Mott transition in wide-band-gap semiconductor quantum wells. *Phys. Rev. B* **90**, 201308 (2014).

39. A. Amo, M. D. Martín, L. Viña, A. I. Toropov, K. S. Zhuravlev, Photoluminescence dynamics in GaAs along an optically induced Mott transition. *J. Appl. Phys.* **101**, 081717 (2007).
40. L. Kappei, J. Szczytko, F. Morier-Genoud, B. Deveaud, Direct observation of the Mott transition in an optically excited semiconductor quantum well. *Phys. Rev. Lett.* **94**, 147403 (2005).
41. D. Bajoni, P. Senellart, E. Wertz, I. Sagnes, A. Miard, A. Lemaître, J. Bloch, Polariton laser using single micropillar GaAs-GaAlAs semiconductor cavities. *Phys. Rev. Lett.* **100**, 047401 (2008).
42. S. Azzini, D. Gerace, M. Galli, I. Sagnes, R. Braive, A. Lemaître, J. Bloch, D. Bajoni, Ultra-low threshold polariton lasing in photonic crystal cavities. *Appl. Phys. Lett.* **99**, 111106 (2011).
43. J. Tatebayashi, S. Kako, J. Ho, Y. Ota, S. Iwamoto, Y. Arakawa, Room-temperature lasing in a single nanowire with quantum dots. *Nat. Photonics* **9**, 501–505 (2015).
44. L. Orosz, F. Réveret, F. Médard, P. Disseix, J. Leymarie, M. Mihailovic, D. Solnyshkov, G. Malpuech, J. Zuniga-Pérez, F. Semond, M. Leroux, S. Bouchoule, X. Lafosse, M. Mexis, C. Brimont, T. Guillet, LO-phonon-assisted polariton lasing in a ZnO-based microcavity. *Phys. Rev. B* **85**, 121201(R) (2012).
45. C. F. Klingshirn, *Semiconductor Optics* (Springer, Berlin, ed. 4, 2012).
46. H.-Y. Li, S. Rühle, R. Khedoe, A. F. Koenderink, D. Vanmaekelbergh, Polarization, microscopic origin, and mode structure of luminescence and lasing from single ZnO nanowires. *Nano Lett.* **9**, 3515–3520 (2009).
47. Y. Ma, X. Guo, X. Wu, L. Dai, L. Tong, Semiconductor nanowire lasers. *Adv. Opt. Photonics* **5**, 216–273 (2013).
48. J. Lagois, Depth-dependent eigenenergies and damping of excitonic polaritons near a semiconductor surface. *Phys. Rev. B* **23**, 5511–5520 (1981).
49. B. Segall, Intrinsic absorption "Edge" in II-VI semiconducting compounds with the Wurtzite structure. *Phys. Rev.* **163**, 769–778 (1967).
50. H. Yoshikawa, S. Adachi, Optical constants of ZnO. *Jpn. J. Appl. Phys.* **36**, 6237–6243 (1997).

Acknowledgments

Funding: This work was supported by the Basic Science Research Program (2016R1A2B4014448 and 2016R1A6A3A11933287) and the Leading Foreign Research Institute Recruitment Program (2018K1A4A3A03075584) through the National Research Foundation of Korea and by the DGIST R&D Program (19-BT-02) funded by the Ministry of Science and ICT of the Korean Government. The work at the University of Pennsylvania was supported by the RAISE-EQuIP-NSF-ECCS-1842612 grant from the NSF (USA). **Author contributions:** J.-W.K. and C.-H.C. conceived the project. J.-W.K. and S.-J.P. fabricated the samples. J.-W.K., W.L., and C.-H.C. conducted the optical measurements. J.-W.K. and B.S. performed the numerical calculations. J.-W.K., R.A., and C.-H.C. analyzed the data and wrote the manuscript, with input from all authors. **Competing interests:** The authors declare that they have no competing interests. **Data and materials availability:** All data needed to evaluate the conclusions in the paper are present in the paper and/or the Supplementary Materials. Readers are welcome to comment on the online version of the paper. Correspondence and requests for materials should be addressed to C.-H.C. (chcho@dgist.ac.kr) or R.A. (riteshag@seas.upenn.edu).

Submitted 29 July 2018
Accepted 1 March 2019
Published 19 April 2019
10.1126/sciadv.aau9338

Citation: J.-W. Kang, B. Song, W. Liu, S.-J. Park, R. Agarwal, C.-H. Cho, Room temperature polariton lasing in quantum heterostructure nanocavities. *Sci. Adv.* **5**, eaau9338 (2019).

Room temperature polariton lasing in quantum heterostructure nanocavities

Jang-Won Kang, Bokyung Song, Wenjing Liu, Seong-Ju Park, Ritesh Agarwal and Chang-Hee Cho

Sci Adv **5** (4), eaau9338.
DOI: 10.1126/sciadv.aau9338